scientific data

Check for updates

OPEN

DATA DESCRIPTOR

Single cell transcriptome profiling of peripheral blood mononuclear cells in Guillain–Barré syndrome patients

Peng Shi[1,3], Yi Diao[1,3], Hui Yang[1], Ronglian Li[1], Ming Ye[1], Dongliang Liu[1,4] & Di Nian[2,4] ✉

Guillain-Barré syndrome (GBS) is an autoimmune disorder characterized by acute peripheral demyelination, leading to progressive muscle weakness and sensory loss. While CD4⁺ T cells and circulating macrophages are implicated in autoimmune neuropathies, the compositional dynamics and activation mechanisms of circulating immune cells remain elusive. Here, we performed single-cell RNA sequencing (scRNA-seq) on peripheral blood mononuclear cells (PBMC) from 3 GBS patients and 2 healthy controls. A total of 51358 cells in the PBMC dataset passed the quality control. In addition, immune cell activation and recruitment were validated using mouse model single-cell datasets and rat transcriptome datasets. We delineate a T-cell differentiation–chemokine secretion axis that operates as a pathogenic hub in inflammatory neuropathy. This data resource provides an indispensable foundation for developing immunomodulatory therapies in Guillain–Barré syndrome.

Background & Summary

Guillain-Barré syndrome (GBS) is an acute autoimmune neuropathy characterized by rapidly progressive limb weakness and sensory disturbances, representing the most frequent cause of acute flaccid paralysis worldwide. Its incidence ranges from 0.4 to 2.5 per 100,000 individuals annually[1–3]. Acute inflammatory demyelinating polyneuropathy (AIDP) and acute motor axonal neuropathy (AMAN) constitute the two most prevalent GBS subtypes. Despite advances with intravenous immunoglobulin (IVIG) and plasma exchange therapies, approximately one-fifth of patients experience severe disability or mortality[4–6], underscoring an urgent need to elucidate the underlying immunopathological mechanisms.

Current evidence supports a model wherein molecular mimicry between microbial antigens (e.g., *Campylobacter jejuni* lipopolysaccharides) and peripheral nerve gangliosides triggers GBS, leading to autoantibody production and complement-mediated nerve damage[7–9]. While animal studies using experimental autoimmune neuritis (EAN) models implicate T cell responses to compact myelin proteins (notably P2 and P0), the dynamic interplay between innate and adaptive immune cells—specifically, the heterogeneity of T cell subsets and their interactions with B cells and other cell types in breaching the blood-nerve barrier to attack myelin—remains poorly understood[10–12].

Pro-inflammatory cytokines, including IL-1β, IL-6, IL-12, TNF-α, and IFN-γ, contribute to myelin damage by recruiting effector cells to peripheral nerves and promoting local release of toxic mediators. Conversely, anti-inflammatory cytokines such as IL-4 and IL-10 suppress disease progression or facilitate myelin repair[13]. Peripheral blood mononuclear cells (PBMCs)—comprising T cells, B cells, monocytes, and dendritic cells—provide a crucial window into systemic immune dysregulation in GBS. Previous bulk studies identified elevated pro-inflammatory cytokines (e.g., IL-17, IFN-γ) in GBS patient PBMCs[13–15], yet these approaches obscure cell type-specific responses and fail to resolve functionally distinct immune subsets driving pathogenesis. Single-cell RNA sequencing (scRNA-seq) has revolutionized the dissection of immune cell heterogeneity and transcriptional states in autoimmune disorders such as multiple sclerosis and lupus[16–18].

[1]Department of Neurology, The First Affiliated Hospital of Bengbu Medical University, Bengbu, 233004, China. [2]Department of Medical Examination, Bengbu Medical University, Bengbu, 233030, China. [3]These authors contributed equally: Peng Shi, Yi Diao. [4]These authors jointly supervised this work: Dongliang Liu, Di Nian. ✉e-mail: 474037315@qq.com; niandi07@sohu.com

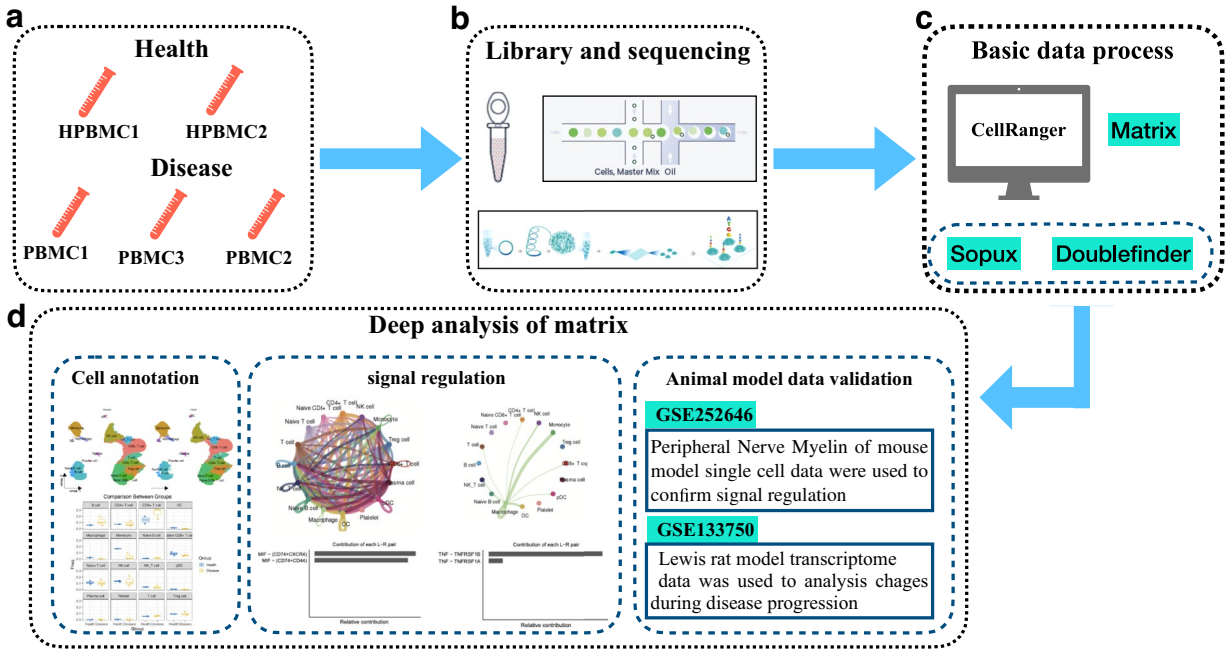

Fig. 1 Graphical representation of the study design and experimental workflow. (**a**) Sample collection and group information. (**b**) Library construction and sequencing schematic diagram. (**c**) Basic data process, including sequencing raw data quality control, Cell Ranger analysis to obtain expression matrices, and filtering out background RNA contamination and double cells. (**d**) Depth analysis is divided into three parts: first, annotation of cell subpopulations; second, analysis of cell interactions and receptor ligands for cell subpopulations; third, single-cell data analysis of animal models and validation of transcriptome data during disease progression.

High-resolution single-cell profiling of peripheral blood from patients with Guillain–Barré syndrome (GBS) remains scarce. Meng Li *et al.* generated scRNA-seq maps of peripheral blood mononuclear cells from five individuals with acute-phase disease and identified a clonally expanded $CD14^{+}+CD163^{+}$ monocyte subset that is transcriptionally wired for IL-1 and chemokine signaling, highlighting a previously unrecognized axis of monocyte heterogeneity in GBS inflammation[19]. A pilot study of treatment-naïve patients with an AIDP variant of GBS who presented with work-related stress plus concurrent enteritis/gastritis revealed concomitant activation of TH1 and TH17 programmed and markedly increased predicted crosstalk between monocytes/macrophages and both Schwann cells and sensory neurons[20]. Recently, work in animal models of inflammatory neuropathy by Maryamsadat Seyedsadr *et al.* pinpointed IL-21 signaling, T-follicular-helper/T-peripheral-helper differentiation and CXCR6-driven T-cell trafficking as central drivers of disease, offering tractable therapeutic targets for GBS[12].

Here, we performed high-resolution scRNA-seq on PBMCs from treatment-naïve GBS patients and matched healthy controls, integrating these data with scRNA-seq from animal models and bulk transcriptomics for technical validation. We uncover a co-stimulatory and mutually reinforcing circuit between pro-inflammatory T-cell subsets and circulating macrophage populations that amplifies peripheral neuroinflammation. Collectively, these data establish peripheral immune cell crosstalk as a pivotal driver of disease progression and identify tractable molecular targets for treating autoimmune peripheral neuropathies. The integrated workflow and conceptual framework presented in Fig. 1 provides a transparent roadmap for future use of this dataset.

Methods

Specimen collection. This study enrolled patients with Guillain-Barré syndrome (GBS) hospitalized at the First Affiliated Hospital of Bengbu Medical University between June and November 2024. Using established diagnostic criteria for GBS[21–23], we included three individuals with the acute inflammatory demyelinating polyneuropathy (AIDP) subtype. Exclusion criteria were as follows: (1) any neuro-autoimmune disorder—multiple sclerosis, neuromyelitis optica spectrum disorder, autoimmune encephalitis or related conditions; (2) chronic metabolic or cardiovascular disease, including type 2 diabetes, metabolic syndrome and established cerebrovascular pathology; (3) surgery within the preceding three months; (4) concurrent infection, heart failure, malignancy or hepatic or renal impairment; and (5) sustained tobacco or alcohol use. Healthy control samples were obtained from age-/sex-matched volunteers undergoing routine health examinations at the same institution and confirmed as medically unremarkable. All participants have signed a written informed consent form, and the research protocol has been approved by the Institutional Review Committee of the First Affiliated Hospital of Bengbu Medical University (Ethics Approval No.: Lunke pizi [2020] No. 107). Supplementary Table S1 showed the sample information.

PBMC isolation and single-cell sequencing. Peripheral blood was collected from enrolled participants in EDTA K_2 tubes. Peripheral blood mononuclear cells (PBMCs) were isolated from whole blood using Mononuclear Cell Separation Solution (Cat: P9011), resuspended in serum-free cryopreservation medium

Ultra (Cat: C2958), and stored at −80 °C. To minimize batch effects, all subsequent procedures were performed simultaneously after sample collection. Cryopreserved cells were thawed, stained with 0.4% trypan blue, and assessed microscopically; only samples with >80% viability was processed for library preparation. Single-cell Gel Bead-In-EMulsions (GEMs, Chromium™ Next GEM Single Cell 3' Kit v3.1, Cat: 1000268) were generated using a Chromium Controller (10x Genomics), followed by in-GEM reverse transcription. cDNA amplification, enzymatic fragmentation, adapter ligation, and index PCR were performed per manufacturer's protocol to construct sequencing libraries. Quality-controlled libraries underwent circularization and were sequenced on a DNBseq-2000 platform (MGI, Shenzhen, China) with 150-bp paired-end reads.

Data quality control and data processing. Raw data were initially processed using fastp (version: 0.24.0) to remove adapters and low-quality reads, yielding clean reads. Subsequently, Cell Ranger (version: 7.2.0) was employed to align these clean reads to the reference genome (Human reference (GRCh38)-2020-A: https://cf.10xgenomics.com/supp/cell-exp/refdata-gex-GRCh38-2020-A.tar.gz), resulting in the generation of an expression matrix. The resultant gene expression matrix was analyzed using R software (version 4.1.1) and the Seurat package (version 4.0.6). To filter out contamination from background RNA, the SoupX package (version: 1.6.2) was utilized[24]. DoubletFinder (version: 2.0.4)[25] was applied to identify and exclude doublet cells. Following this, cell cycle calculations were performed, and mitochondrial, hemoglobin, and ribosomal genes were filtered out. The cleaned cell expression matrix was then subjected to dimensionality reduction and clustering analyses using standard workflows within the Seurat package.

Cell annotation. The FindAllMarkers function, employing the Wilcoxon rank-sum test, was utilized to identify specific markers for all clusters. The calculation parameters were set as follows: only.pos = TRUE, min.pct = 0.25, and logfc.threshold = 0.25. Initial cell annotations were performed using the easybio package (version 1.1.1), which were subsequently manually curated. Additionally, the artificial intelligence model deepseek-reasoner (DeepSeek R1) was employed for inferential annotation. The final cell annotations were derived by integrating results from both manual curation and annotations generated by the easybio package, alongside insights from deep seek-reasoner.

Cell interaction and pseudotemporal analysis. The CellChat package (version 2.1.2) was utilized for analyzing cell-cell interactions. This involved selecting a curated database of secreted ligands and receptors to compute interaction intensities and analyze cell interaction networks. The results were visualized using network and bubble plots. Pseudotime analysis, also known as trajectory analysis, was performed using monocle3 (version 1.3.7). This software was employed to analyze cellular pseudotime, allowing for the calculation of differentiation times for each cell subpopulation based on a presumed starting point of cellular differentiation.

Analysis of transcription factors and signaling pathways. Transcriptional regulator and pathway activity were simultaneously inferred using decoupleR (v2.10.0). This algorithm integrates signed directed networks with weighted interactions from curated databases to model context-specific biological activity changes, providing computational resolution of transcription factor regulation, kinase-substrate signaling networks, and related mechanistic pathways.

External data acquisition and processing. Single-cell sequencing data GSE252646 (mouse model) and GSE133750 (rat neural tissue) were retrieved from the Gene Expression Omnibus. Bulk transcriptome differential expression analysis employed limma (v3.62.2), with scRNA-seq data processed identically to the PBMC analytical pipeline. STEM (Short Time-series Expression Miner) was used to analyze genes that are specifically overexpressed as the disease progresses by using the OECloud tools at https://cloud.oebiotech.com.

Data Records

The single cell transcriptomic raw sequencing data (fastq files) were deposited in can be found in NCBI SRA database with accession number PRJNA1293757(https://www.ncbi.nlm.nih.gov/bioproject/PRJNA1293757)[26]. The mouse single-cell sequencing dataset were from GEO database (accession number: GSE252646)[27]. The rat neural tissue transcriptomic datasets were from GEO database (accession number: GSE133750)[28]. The cellranger output files, the rds and Rdata files of $CD4^+$ T cells, $CD8^+$ T cells and circulating macrophages, STEM files of rat model have been uploaded to Mendeley Data, with the following DOIs and corresponding URLs: cellranger output files of PRJNA1293757, https://doi.org/10.17632/f2523nkt3m.2 (https://data.mendeley.com/datasets/f2523nkt3m/2)[29]; rds and Rdata files of CD4 + T cells, CD8 + T cells and circulating macrophages, https://doi.org/10.17632/xfszbc93cy.2 (https://data.mendeley.com/datasets/xfszbc93cy/2)[30]; STEM files of rat model, https://doi.org/10.17632/yxd283n6xf.2 (https://data.mendeley.com/datasets/yxd283n6xf/2)[31]; cellranger output files of mouse model, https://doi.org/10.17632/dsf5rxk8z6.1 (https://data.mendeley.com/datasets/dsf5rxk8z6/1)[32].

Technical Validation

The quality control of scRNAseq data. Raw sequencing data processed using Cell Ranger have been deposited in the Mendeley Data repository (https://doi.org/10.17632/f2523nkt3m.2). Initial quality assessment revealed: Valid barcode detection: 95.6–96.6%; Genome mapping efficiency: 91.4–97.1%; Median genes detected per cell: 1701–2158. Pre-filtered datasets contained 9,044–12,703 cells per sample (aggregate n = 57,887 across 5 samples). Rigorous quality control was performed through: 1. Ambient RNA removal; 2. Doublet exclusion (Fig. 2b–f); 3. Threshold-based filtration by Cell counts, Gene detection and Mitochondrial content (Fig. 2a); 4.

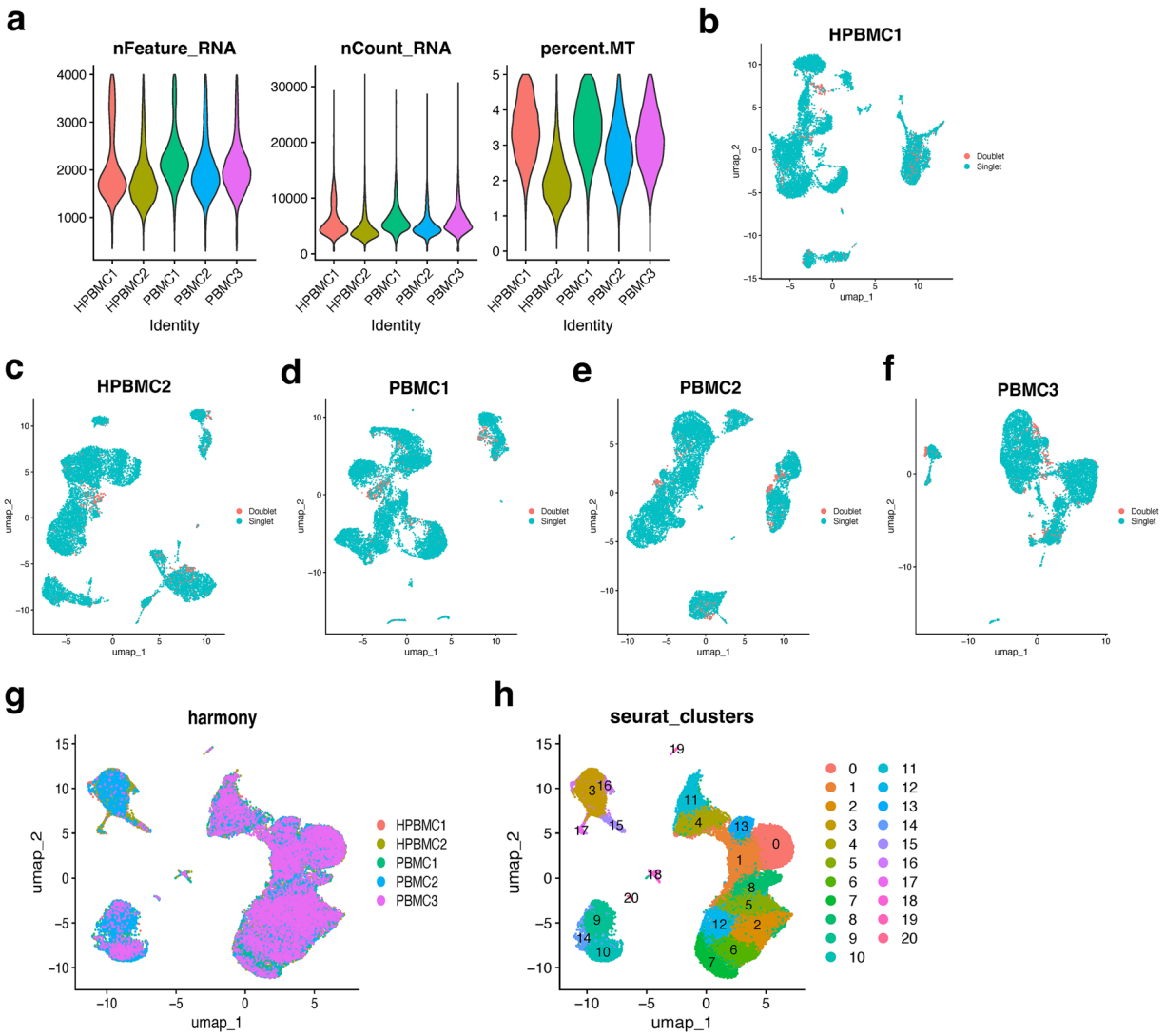

Fig. 2 The quality control of scRNAseq data. (**a**) Violin plot of nFeature_RNA, nCount_RNA and percent.MT after filtered. (**b**–**f**) The UMAP of double and single cells about each sample. (**g**) The UMAP of integrate each sample matrix by harmony. (**h**) The UMAP of non-linear dimensional reduction.

Exclusion of ribosomal and hemoglobin transcripts. Post-QC datasets retained 51,358 high-quality cells. Batch correction using Harmony successfully integrated samples, with cluster convergence validated in Fig. 2g.

The annotation of each cluster. Initial clustering using canonical PBMC marker genes (Fig. 3a, with complete gene list in Fig. 3b) revealed distinct immune cell populations. Population distributions across samples were quantified (Fig. 3c), demonstrating consistent cellular composition patterns. Through refined sub-clustering analysis with CellMarker 2.0 database (processed via easyBio software), we identified 16 functionally distinct subsets (Fig. 3d). Notably, disease-associated circulating macrophages - a rare population of tissue-derived macrophages in peripheral blood – constituted <1% of total cells (Fig. 3e). Complete cellular abundance data are provided in Supplementary Table S2.

The annotation of T cell sub-celltype. Following meticulous cell annotation, we isolated $CD4^+$ and $CD8^+$ T cell subsets for dimensional reduction and sub-clustering analysis (Fig. 4a,c). Disease cohorts exhibited significant expansion of activated $CD4^+$ T cells and effector memory $CD8^+$ T cell populations (Fig. 4b,d), consistent with the immunopathological microenvironment in autoimmune disorders. During sub-clustering of the $CD4^+$ T cells we noted a minor population that expressed canonical $CD8^+$ T-cell signatures; conversely, two subsets within the $CD8^+$ compartment resisted definitive annotation and were labelled Mix1 and Mix2. These artefacts do not influence downstream functional analyses. Pseudo temporal reconstruction then delineated the inferred differentiation trajectories of both $CD4^+$ and $CD8^+$ T-cell subsets (Fig. 4e,f), with temporally resolved expression profiles of key signature genes provided in Fig. 4g,h.

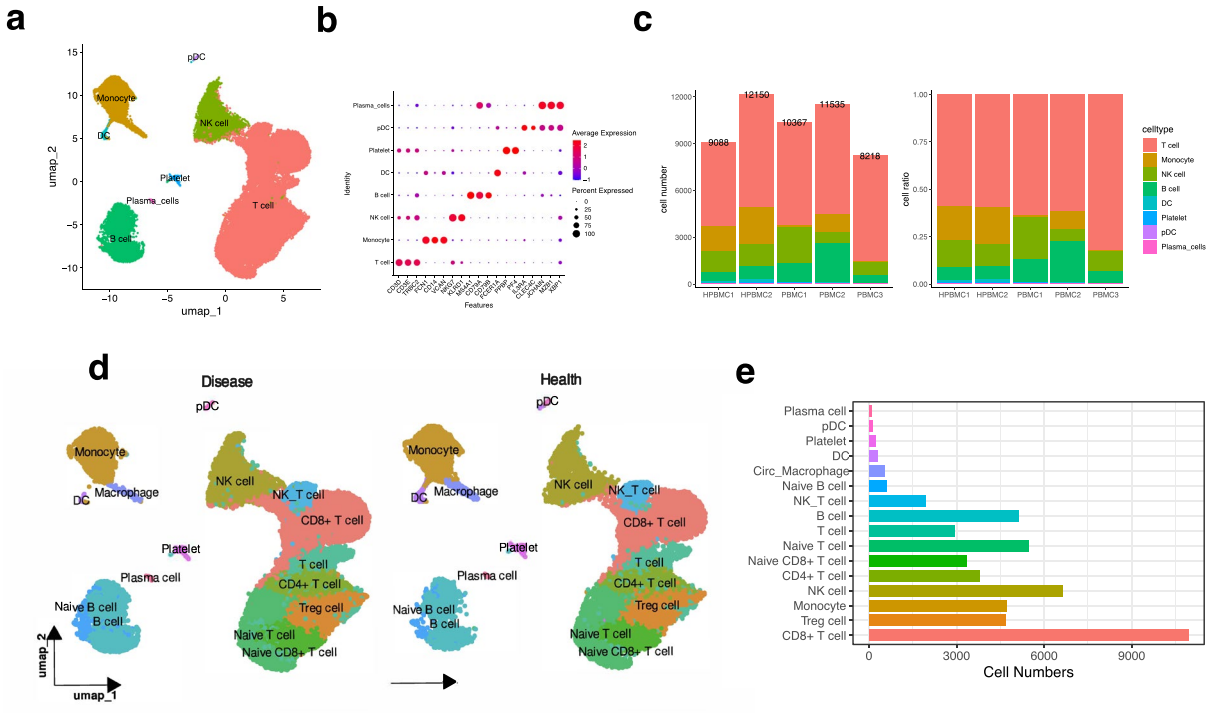

Fig. 3 The annotation of each cluster. (**a**) The UMAP of main type cell annotation. (**b**) The dotplot of marker genes in cell types, the size of dot represented the percent gene expression of each cell types, the color represented the expression of gene expression. (**c**) The histogram of cell number and cell ratio in each sample. (**d**) The UMAP of detailed cell annotation of health and disease group. (**e**) The bar chart of cell number about every cell types.

The annotation of circulating macrophages. Re-clustering and re-annotation of circulating macrophages (Circ_Macrophage) revealed their resistance to conventional M0/M1/M2 classification. We therefore defined eight Circ_Macrophage subpopulations based on functional characteristics of the top 10 highly expressed genes (Fig. 5a–c), including apoptosis-related, immune-regulatory, and inflammation-activated subsets. Notably, we identified a T cell-contaminated population (expressing canonical T cell markers: CD247, TRAC, ITK) that was excluded from subsequent analyses. KEGG and GO enrichment analyses demonstrated that immune-regulatory and inflammation-activated subpopulations directly modulate immunoregulatory and pro-inflammatory pathways, respectively (Fig. 5d–g). These molecularly defined subsets provide foundational insights into how circulating macrophages participate in autoimmune pathogenesis.

The cell-cell interaction and molecular regulation. Single cell sequencing not only delineates the immune cell landscape but also deciphers molecular interaction patterns between distinct cell populations, providing critical insights into intercellular crosstalk and immune regulation. Our technical validation were as follows: a comprehensive cellular regulatory network across immune subsets (Fig. 6a); Dominant receptor-ligand pairs mediating $CD4^+/CD8^+$ T cell interactions, with MIF-(CD74 + CXCR4) and MIF-(CD74 + CD44) showing particularly strong engagement (Fig. 6b,d); TNF signaling as the primary pathway for Circ_Macrophage communication (Fig. 6c,e); MIF-mediated signaling in $CD4^+$ T cells triggering downstream CCL and IL16 pathway activation upon feedback reception, thereby potentiating immune responses (Fig. 6g).

Single-cell RNA sequencing of sciatic nerves from NOD.AireGW/- mice revealed prominent macrophage-immune cell interactions mediated by CXCL signaling pathways (Fig. 6h), with chemokine ligand-receptor pairs showing particularly strong involvement (Fig. 6i). Notably, TNF signaling emerged as a highly specific pathway governing these neuroimmune cross-talks (Fig. 6j). Transcriptomic analysis of Lewis rat sciatic nerves during experimental autoimmune neuritis progression identified persistently elevated expression of key inflammatory genes (Fig. 6k, Supplementary Table S3). KEGG pathway analysis of these core genes highlighted enrichment in: NF-κB cytokine signaling, Inflammatory Th1 differentiation, Ligand-receptor interactions, Chemokine/cytokine networks (Fig. 6l), These chemokine-related genes maintained sustained high expression throughout disease progression (Fig. 6m), suggesting their crucial role in chronic inflammatory responses.

We established a high-quality single-cell transcriptomic atlas of peripheral blood mononuclear cells in Guillain-Barré syndrome (GBS), achieving robust cell-type annotation and revealing disease-specific cellular interactions. Complementary studies in NOD.AireGW/- mice and Lewis rats further delineated the immune cell

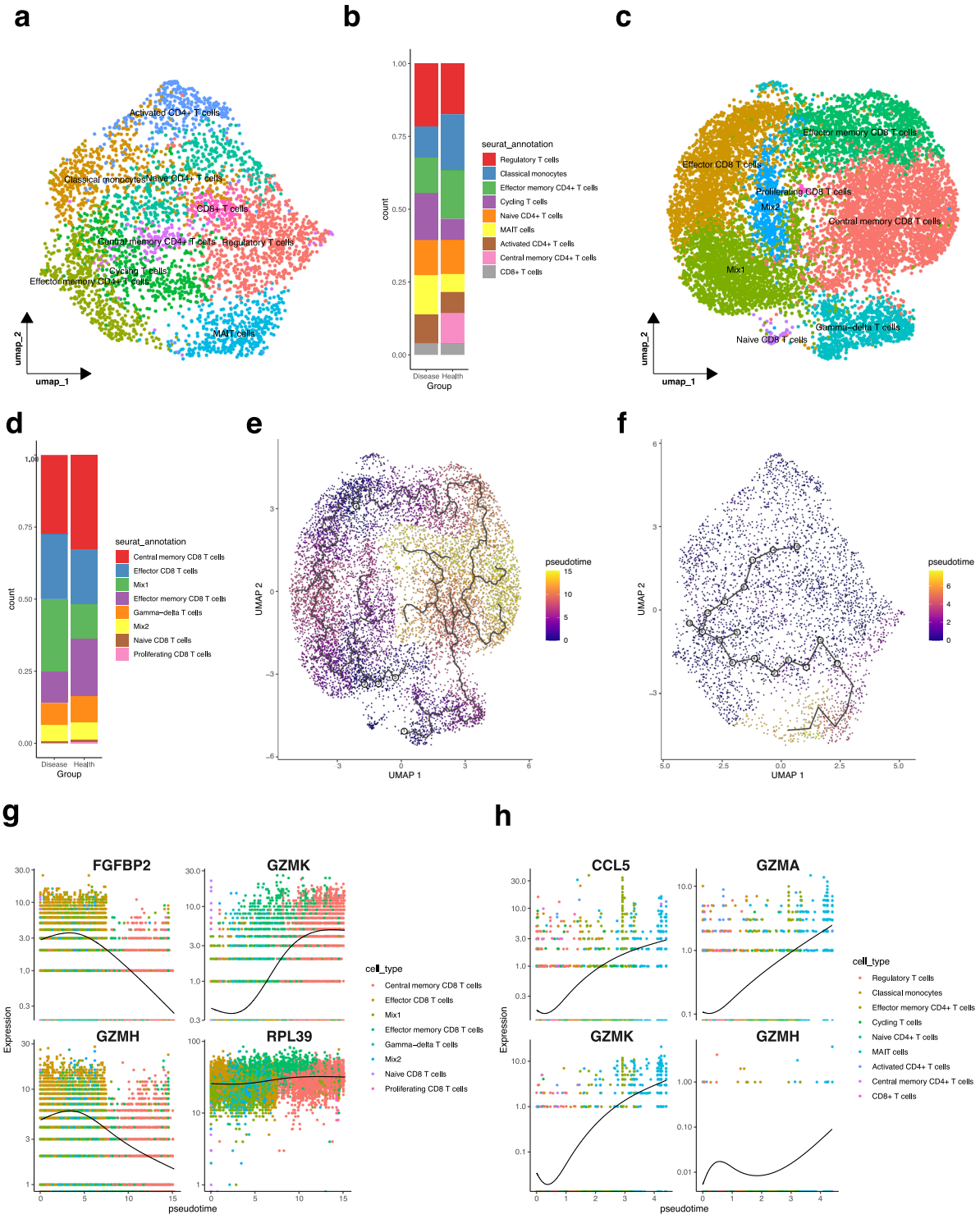

Fig. 4 The annotation of T cell sub-cell types. (**a**) The UMAP of CD4 + T cells. (**b**) The histogram of cell-ratio in each group. (**c**) The UMAP of CD8 + T cells. (**d**) The histogram of cell-ratio in each group. (**e**) and (**f**) The UMAP of pseudotime about CD8 + T cells and CD4 + T cells. (**g**) and (**h**) Expression of key genes along the monocle3 pseudotime trajectory.

dynamics and signaling pathways underlying GBS pathogenesis. This comprehensive dataset provides a foundational resource for investigating aberrant immune activation and intercellular crosstalk in the acute inflammatory demyelinating polyneuropathy (AIDP) subtype of GBS.

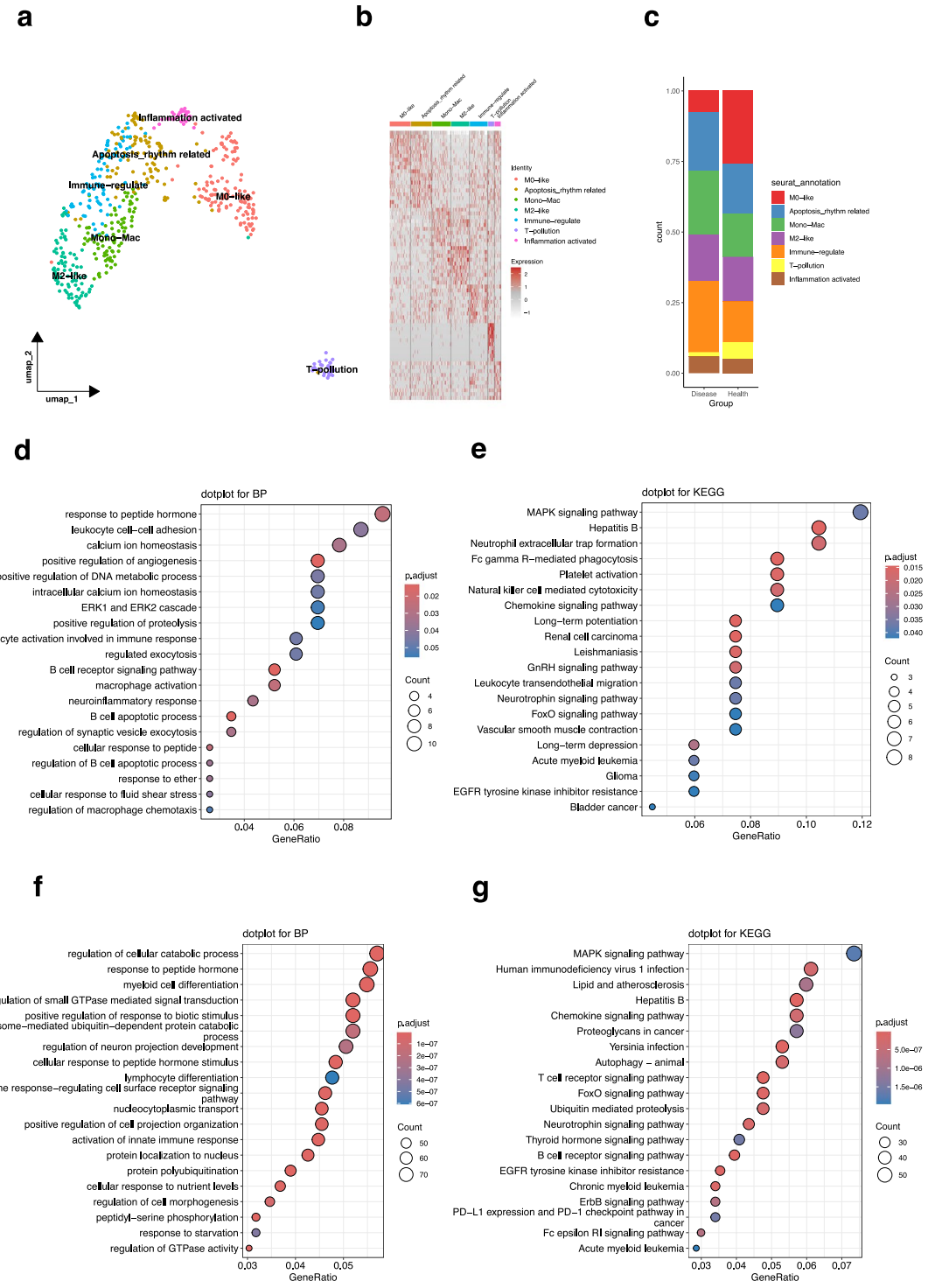

Fig. 5 The annotation of circulating macrophages. (**a**) The UMAP of each cell type. (**b**) The heatmap of marker-genes in each cell type. (**c**) The histogram of cell-ratio in each group. (**d**) The dotplot of GO enrichment in bioprocess term about immune-regulate cells. (**e**) The dotplot of KEGG enrichment about immune-regulate cells. (**f**) The dotplot of GO enrichment in bioprocess term about Inflammation activated cells. (**g**) The dotplot of KEGG enrichment about Inflammation activated cells.

Data availability

The scRNA seq data processing pipeline runs on the Linux operating system. All R source code used for downstream data analysis and visualization is provided online (https://github.com/shuaifengwang/scRNAseq-of-PBMC-in-Guillain-Barr-syndrome)[33]. The raw data of single-cell sequencing can be found in the SRA database (https://www.ncbi.nlm.nih.gov/bioproject/PRJNA1293757)[26]. The details of the files used in the article have been described in the "data records" section.

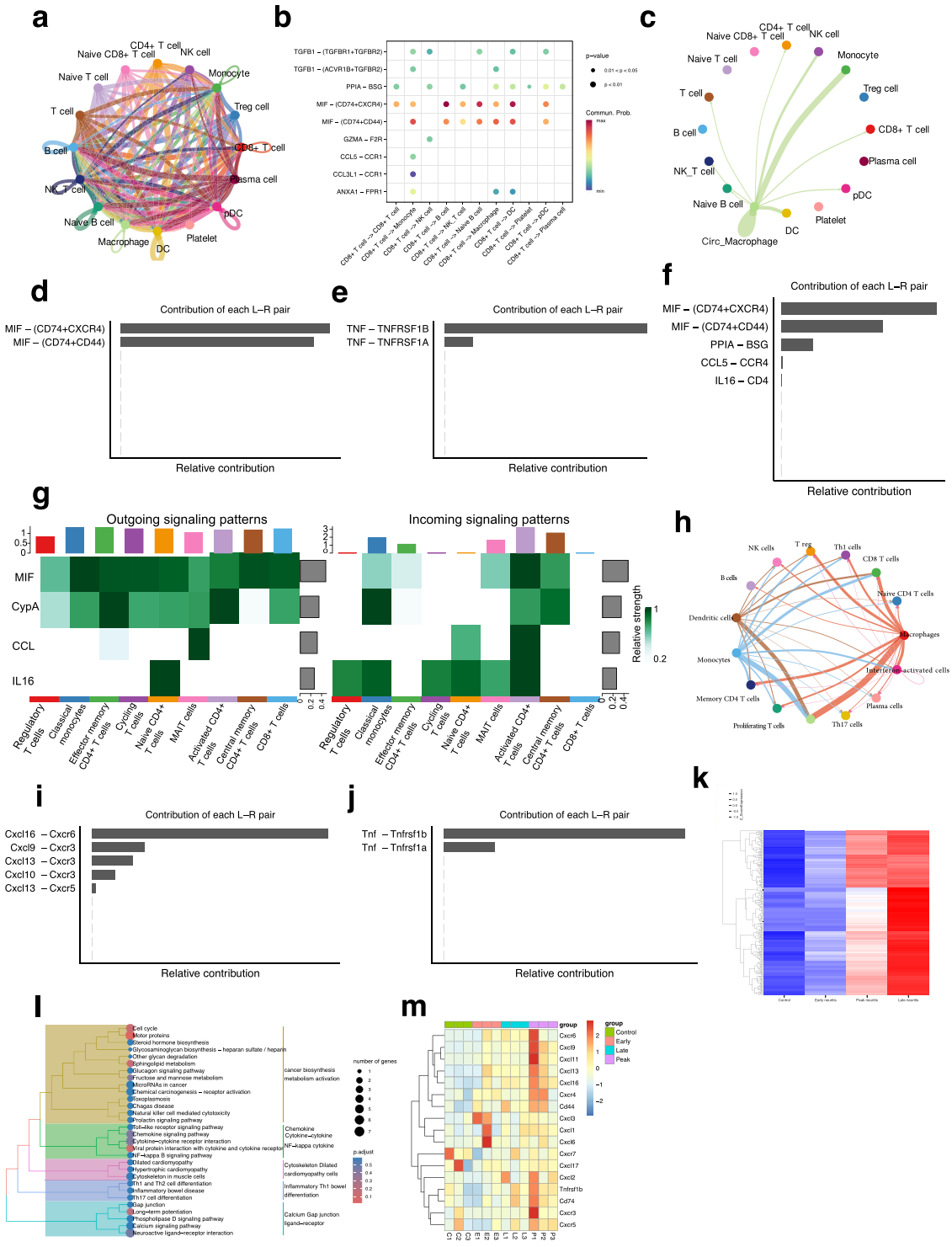

Fig. 6 The cell-cell interaction and molecular regulation. (**a**) The network of interaction between collotypes. (**b**) The interaction between myeloid cells, CD4 + T cells and CD8 + T cells. (**c**) The network of interaction between Circ_Macrophage and other cell types. (**d**) Relative contribution of MIF-(CD74 + CXCR4) and MIF-(CD74 + CD44) in disease group. (**e**) Relative contribution of MTNF-TNFRSF1B and TNF-TNFRSF1A in disease group. (**g**) The Outgoing signaling patterns and Incoming signaling patterns in each CD4 + T cell types. (**h**) CellChat analysis of ligand-receptor interactions shows upregulation of the CXCL pathway. (**i**) Relative contribution of chemokine L-R pairs in the sciatic nerves of NOD.AireGW/- mice. (**j**) Relative contribution of Tnf-Tnfrsf1b, Tnf-Tnfrsf1a in disease group. (**k**)The heatmap of continuously overexpressing genes during the progression of the disease in rat model. (**l**) KEGG enrichment of continuously overexpressing genes during the progression of the disease in rat model. (**m**) The heatmap of chemokine expression during the progression of the disease in rat model.

Code availability

All software used for technical validation is detailed in the Methods. Code for single-cell data processing—encompassing ambient RNA removal, doublet filtering, batch correction, cell annotation and downstream validation—is available at link: https://github.com/shuaifengwang/scRNAseq-of-PBMC-in-Guillain-Barr-syndrome[33].

Received: 4 August 2025; Accepted: 20 May 2026;
Published online: 05 June 2026

References

1. Cheng, Q. *et al*. Distinct pattern of age-specific incidence of Guillain-Barre syndrome in Harbin, China. *J Neurol* **249**, 25–32, https://doi.org/10.1007/pl00007844 (2002).
2. Islam, Z. *et al*. High incidence of Guillain-Barre syndrome in children, Bangladesh. *Emerg Infect Dis* **17**, 1317–1318, https://doi.org/10.3201/eid1707.102031 (2011).
3. De la Cruz-Mosso, U. *et al*. MIF promotes a differential Th1/Th2/Th17 inflammatory response in human primary cell cultures: Predominance of Th17 cytokine profile in PBMC from healthy subjects and increase of IL-6 and TNF-alpha in PBMC from active SLE patients. *Cell Immunol* **324**, 42–49, https://doi.org/10.1016/j.cellimm.2017.12.010 (2018).
4. Yuki, N. & Hartung, H. P. Guillain-Barre syndrome. *N Engl J Med* **366**, 2294–2304, https://doi.org/10.1056/NEJMra1114525 (2012).
5. van den Berg, B. *et al*. Guillain-Barre syndrome: pathogenesis, diagnosis, treatment and prognosis. *Nat Rev Neurol* **10**, 469–482, https://doi.org/10.1038/nrneurol.2014.121 (2014).
6. Goodfellow, J. A. & Willison, H. J. Guillain-Barre syndrome: a century of progress. *Nat Rev Neurol* **12**, 723–731, https://doi.org/10.1038/nrneurol.2016.172 (2016).
7. Jacobs, B. C. *et al*. The spectrum of antecedent infections in Guillain-Barre syndrome: a case-control study. *Neurology* **51**, 1110–1115, https://doi.org/10.1212/wnl.51.4.1110 (1998).
8. Cao-Lormeau, V. M. *et al*. Guillain-Barre Syndrome outbreak associated with Zika virus infection in French Polynesia: a case-control study. *Lancet* **387**, 1531–1539, https://doi.org/10.1016/S0140-6736(16)00562-6 (2016).
9. Islam, Z. *et al*. Axonal variant of Guillain-Barre syndrome associated with Campylobacter infection in Bangladesh. *Neurology* **74**, 581–587, https://doi.org/10.1212/WNL.0b013e3181cff735 (2010).
10. Linington, C. *et al*. A permanent rat T cell line that mediates experimental allergic neuritis in the Lewis rat *in vivo*. *J Immunol* **133**, 1946–1950 (1984).
11. Linington, C., Lassmann, H., Ozawa, K., Kosin, S. & Mongan, L. Cell adhesion molecules of the immunoglobulin supergene family as tissue-specific autoantigens: induction of experimental allergic neuritis (EAN) by P0 protein-specific T cell lines. *Eur J Immunol* **22**, 1813–1817, https://doi.org/10.1002/eji.1830220721 (1992).
12. Seyedsadr, M. *et al*. A pathologically expanded, clonal lineage of IL-21-producing CD4+ T cells drives inflammatory neuropathy. *J Clin Invest* **134**. https://doi.org/10.1172/JCI178602 (2024).
13. Lu, M. O. & Zhu, J. The role of cytokines in Guillain-Barre syndrome. *J Neurol* **258**, 533–548, https://doi.org/10.1007/s00415-010-5836-5 (2011).
14. Wu, X., Wang, J., Liu, K., Zhu, J. & Zhang, H. L. Are Th17 cells and their cytokines a therapeutic target in Guillain-Barre syndrome? *Expert Opin Ther Targets* **20**, 209–222, https://doi.org/10.1517/14728222.2016.1086751 (2016).
15. Harness, J. & McCombe, P. A. Increased levels of activated T-cells and reduced levels of CD4/CD25+ cells in peripheral blood of Guillain-Barre syndrome patients compared to controls. *J Clin Neurosci* **15**, 1031–1035, https://doi.org/10.1016/j.jocn.2007.09.016 (2008).
16. Schafflick, D. *et al*. Integrated single cell analysis of blood and cerebrospinal fluid leukocytes in multiple sclerosis. *Nat Commun* **11**, 247, https://doi.org/10.1038/s41467-019-14118-w (2020).
17. Nehar-Belaid, D. *et al*. Mapping systemic lupus erythematosus heterogeneity at the single-cell level. *Nat Immunol* **21**, 1094–1106, https://doi.org/10.1038/s41590-020-0743-0 (2020).
18. Perez, R. K. *et al*. Single-cell RNA-seq reveals cell type-specific molecular and genetic associations to lupus. *Science* **376**, eabf1970, https://doi.org/10.1126/science.abf1970 (2022).
19. Li, M. *et al*. Single-cell analysis reveals novel clonally expanded monocytes associated with IL1beta-IL1R2 pair in acute inflammatory demyelinating polyneuropathy. *Sci Rep* **13**, 5862, https://doi.org/10.1038/s41598-023-32427-5 (2023).
20. O'Brien, J. A. *et al*. Peripheral nerve-targeting and pain-promoting transcriptomic signatures in early Guillain-Barré syndrome. *bioRxiv*, 2025.2009.2024.678413. https://doi.org/10.1101/2025.09.24.678413 (2025).
21. Hadden, R. D. *et al*. Electrophysiological classification of Guillain-Barre syndrome: clinical associations and outcome. Plasma Exchange/Sandoglobulin Guillain-Barre Syndrome Trial Group. *Ann Neurol* **44**, 780–788, https://doi.org/10.1002/ana.410440512 (1998).
22. Tan, C. Y., Razali, S. N. O., Goh, K. J. & Shahrizaila, N. Diagnosis of Guillain-Barre syndrome and validation of the Brighton criteria in Malaysia. *J Peripher Nerv Syst* **25**, 256–264, https://doi.org/10.1111/jns.12398 (2020).
23. Scarpino, M. *et al*. Diagnostic accuracy of neurophysiological criteria for early diagnosis of AIDP: A prospective study. *Neurophysiol Clin* **46**, 35–42, https://doi.org/10.1016/j.neucli.2015.12.008 (2016).
24. Young, M. D. & Behjati, S. SoupX removes ambient RNA contamination from droplet-based single-cell RNA sequencing data. *Gigascience* **9**. https://doi.org/10.1093/gigascience/giaa151 (2020).
25. McGinnis, C. S., Murrow, L. M. & Gartner, Z. J. DoubletFinder: Doublet Detection in Single-Cell RNA Sequencing Data Using Artificial Nearest Neighbors. *Cell Syst* **8**, 329–337 e324, https://doi.org/10.1016/j.cels.2019.03.003 (2019).
26. *SRA*. https://www.ncbi.nlm.nih.gov/bioproject/PRJNA1293757 (2025).
27. Seyedsadr, M. *et al*. A pathologically expanded, clonal lineage of IL-21 producing CD4+ T cells drives Inflammatory neuropathy. *bioRxiv*, 2024.2001.2007.574553. https://doi.org/10.1101/2024.01.07.574553 (2024).
28. Xue, Y., Yin, P., Li, G. & Zhong, D. Transcriptomes in rat sciatic nerves at different stages of experimental autoimmune neuritis determined by RNA sequencing. *Clin Exp Immunol* **198**, 184–197, https://doi.org/10.1111/cei.13354 (2019).
29. Shi, P. *The cellranger files of all samples*. https://data.mendeley.com/datasets/f2523nkt3m/2 (2025).
30. Shi, P. *The rds and Rdata files were derived from analyzing cell annotated*. https://data.mendeley.com/datasets/xfszbc93cy/2 (2025).
31. Shi, P. *The intermediate files of rat model*. https://data.mendeley.com/datasets/yxd283n6xf/2 (2025).
32. Shi, P. *The single cell RNAseq data matrix of mouse model GSE252646*. https://data.mendeley.com/datasets/dsf5rxk8z6/1 (2025).
33. *Github*. https://github.com/shuaifengwang/scRNAseq-of-PBMC-in-Guillain-Barr-syndrome (2025).

Acknowledgements

This work was supported by Anhui Provincial Key R&D Programmes (No: 202304295107020075), Natural Science Research Project of Anhui Educational Committee's Major Project (No. KJ2021ZD0084) and 2024 Domestic Visiting Research Fund for Young Key Teachers (JNFX2024039). This work was supported by Anhui Province Key Laboratory of Basic and Translational Research of Inflammation-related Diseases. In addition, the authors would also like to thank the Henan Pentose Biotech Co, Ltd (Henan, China) for the technical support for the single cell analysis.

Author contributions

S.P., D.Y., Y.H., L.R.L., Y.M.G. and L.D.L. conducted experiments and acquired data. M.S., M.F.B., E.C.M., S.Z., H.C.C., M.M. and W.H. analyzed data. N.D. and S.P. provided Giants fund. Mxx, S.P. wrote the manuscript and all authors have approved the version of the manuscript submitted for publication.

Competing interests

The authors declare no competing interests.

Additional information

Supplementary information The online version contains supplementary material available at https://doi.org/10.1038/s41597-026-07489-5.

Correspondence and requests for materials should be addressed to D.N.

Reprints and permissions information is available at www.nature.com/reprints.

Publisher's note Springer Nature remains neutral with regard to jurisdictional claims in published maps and institutional affiliations.